Published in final edited form as:
NMR Biomed. 2011 December ; 24(10): 1216–1225. doi:10.1002/nbm.1677.

A lanthanide complex with dual biosensing properties: CEST and BIRDS with EuDOTA-(gly)$_4^{-}$

Daniel Coman[‖,§,*], **Garry E. Kiefer**[†], **Douglas L. Rothman**[‖,§,*,‡], **A. Dean Sherry**[+,$], and **Fahmeed Hyder**[‖,§,*,‡]

[‖]Magnetic Resonance Research Center (MRRC), Yale University, New Haven, CT, USA

[§]Core Center for Quantitative Neuroscience with Magnetic Resonance (QNMR), Yale University, New Haven, CT, USA

[*]Department of Diagnostic Radiology, Yale University, New Haven, CT, USA

[‡]Department of Biomedical Engineering, Yale University, New Haven, CT, USA

[†]Macrocyclics, Dallas, TX, USA

[+]Advanced Imaging Research Center and Department of Radiology, University of Texas Southwestern Medical Center, Dallas, TX, USA

[$]Department of Chemistry, University of Texas, Dallas, TX, USA

Abstract

Responsive contrast agents (RCAs) [R1.12] composed of lanthanide III ion (Ln^{3+}) complexes with a variety of 1,4,7,10-tetraazacyclododecane-1,4,7,10-tetraacetate ($DOTA^{4-}$) derivatives have shown great potential as molecular imaging agents for magnetic resonance (MR). A variety of LnDOTA-tetraamide complexes have been demonstrated as RCAs for molecular imaging with ***c***hemical ***e***xchange ***s***aturation ***t***ransfer (CEST). The CEST method detects proton exchange between bulk water and any exchangeable sites on the ligand itself or an inner sphere of bound water that is shifted by a paramagnetic Ln^{3+} bound in the core of the macrocycle. It has also been shown that molecular imaging is possible when the RCA itself is observed (i.e., not its affect on bulk water) using a method called ***b***iosensor ***i***maging of ***r***edundant ***d***eviation in ***s***hifts (BIRDS). The BIRDS method utilizes redundant information stored in the non-exchangeable proton resonances emanating from the paramagnetic RCA for ambient factors like temperature and/or pH. Thus CEST and BIRDS rely on exchangeable and non-exchangeable protons, respectively, for biosensing. We posited that it is feasible to combine these two biosensing features into the same RCA (i.e., dual CEST and BIRDS properties). A complex between europium ion (Eu^{3+}) and DOTA-tetra-glycinate (DOTA-$(gly)_4^{4-}$) is used to demonstrate that its CEST characteristics are preserved while BIRDS properties are detected. In vitro temperature sensitivity of EuDOTA-$(gly)_4^{-}$ is used to show that qualitative MR contrast with CEST can be calibrated using quantitative MR mapping with BIRDS, thereby enabling quantitative molecular imaging at high spatial resolution.

Keywords

amide protons; DIACEST; hydroxyl protons; methyl protons; PARACEST; pH; temperature

Correspondence and reprint requests to: D.S. Fahmeed Hyder / Daniel Coman, N135 TAC (MRRC), 300 Cedar Street, Yale University, New Haven, CT 06520, USA, Tel: +1-203-785-6205, Fax: +1-203-785-6643, fahmeed.hyder@yale.edu / daniel.coman@yale.edu.

Introduction

Paramagnetic complexes are widely used as magnetic resonance imaging (MRI) contrast agents in clinical medicine. These agents – many of which are composed of lanthanide III ion (Ln^{3+}) with a 1,4,7,10-tetraazacyclododecane-1,4,7,10-tetraacetate ($DOTA^{4-}$) backbone – generate contrast by affecting the bulk water proton relaxation rate. However this approach often lacks sensitivity and/or specificity for tracking diseases since the contrast is always "on" when the agent is present. Imaging of specific ions or metabolites is becoming possible with MRI probes, either endogenous or exogenous, which contain exchangeable protons (1,2). The ***c***hemical ***e***xchange ***s***aturation ***t***ransfer (CEST) technique detects exchange between bulk water protons and amide (i.e., $-NH_x$ where x = 1 or 2) or hydroxyl (i.e., -OH) protons in diamagnetic molecules, whereas in paramagnetic molecules the exchangeable pool is either any exchangeable sites on the ligand itself or protons of an inner sphere of bound water that is significantly shifted by Ln^{3+} in the agents' core. The CEST method has tremendous translational potential because it amplifies detection of extracellular targets present at μM to mM level. A great appeal for biomedical imaging is that CEST contrast, either with diamagnetic or paramagnetic agents, can be switched "on" or "off" with a radio-frequency (RF) saturation pulse.

From the earliest days of magnetic resonance spectroscopy (MRS), exchange between bulk solvent water protons (10^1–10^2 M) and bound solute protons (10^{-3}–10^{-2} M) have long been studied using saturation transfer techniques (see ref. (3) for details). CEST with endogenous diamagnetic molecules (e.g., sugars or proteins) is now commonly called DIACEST. Because the chemical shift of a typical diamagnetic exchangeable proton is within a few ppm of bulk water protons, accounting for off-resonance direct saturation of bulk water, indirect saturation via water tightly bound to macromolecules, and poor static magnetic field (B_o) homogeneity are matters that complicate in vivo DIACEST imaging. To help circumvent these problems, in part, a class of paramagnetic CEST probes consisting of a Ln^{3+} bound in a DOTA-tetraamide core, called PARACEST agents, were synthesized to increase the chemical shift separation ($>10^n$ ppm, where $n \geq 1$) between the signals arising from a pool of exchangeable protons of an inner sphere of bound water and bulk solvent water (4,5). This approach allows tuning of water exchange kinetics by choice of chelate structure and/or Ln^{3+} to improve the CEST contrast (2,6). Some PARACEST agents contain bound water molecules with a lifetime in the microseconds range (7). To date, exogenous PARACEST agents have been used to measure various physiological parameters, e.g., pH (5), temperature (8,9), lactate (10), glucose (11,12). Moreover, quantification of physiologically relevant metal ions – e.g., calcium (13) and zinc (14) – were achieved by relaxivity changes of these types of agents. Furthermore, preliminary toxicity studies of prototypical PARACEST agents have shown them to be chemically inert in animals so moving these toward clinical approval is quite conceivable in the near future (15).

Various PARACEST-like agents have been characterized beyond their affects on bulk water relaxation rate or proton exchange. Many have been differentiated in terms of their structure, conformation, and relaxation properties (16,17), thermodynamics, protonation and coordination to alkali metals (18), stability, biodistribution and toxicity (19), as well as sensitivities of non-exchangeable nuclei to ambient factors like temperature and/or pH (20). Previous attempts at biosensing of temperature and/or pH in animal brain by direct detection of Ln^{3+}-based agents may have failed (21) due to very low B_o, poor gradient performance, and/or unfamiliarity with the agents' relaxation properties. More recently with modern technology overcoming these factors have enabled biosensing of temperature and/or pH (22) by a technique termed ***b***iosensor ***i***maging of ***r***edundant ***d***eviation in ***s***hifts (BIRDS) (23,24). The BIRDS method utilizes the redundant information stored in chemical shifts emanating from the paramagnetic Ln^{3+}-based agent for ambient factors like temperature and/or pH. To

date, mainly the agents' non-exchangeable proton resonances (i.e., -CH_x) have been measured, but all other observable nuclei (^{17}O, ^{15}N, ^{13}C, ^{31}P) are equally viable candidates for BIRDS. Superior temperature and/or pH sensitivities of proton chemical shifts emanating from two thulium III ion (Tm^{3+}) containing macrocyclics – 1,4,7,10-tetraazacyclododecane-1,4,7,10-tetrakis(methylene phosphonate) (or $DOTP^{8-}$) and 1,4,7,10-tetramethyl 1,4,7,10-tetraazacyclodoecane-1,4,7,10-tetraacetate (or $DOTMA^{4-}$) – have been demonstrated in rat brain with BIRDS (23,24). Generally, agents with BIRDS properties stand in contrast to PARACEST agents by the fact that in the latter only the [R1.A] effect on bulk water is detected whereas in the former the agent itself is detected. This enables BIRDS to be more quantitative than CEST, but it has much lower spatial resolution. Since the relative advantages and disadvantages of BIRDS and CEST do not apparently overlap, it is tantalizing to consider a new family of agents that perhaps combines these two properties.

Since CEST and BIRDS methods differ respectively by their dependence on exchangeable and non-exchangeable protons for biosensing, we conjectured whether these two features can be supported on the same agent for improved biosensing with dual CEST and BIRDS properties. To test this end, we chose a complex between the europium ion (Eu^{3+}) and a tetraglycinate derivative of $DOTA^{-4}$, EuDOTA-$(gly)_4^-$, which has been previously characterized as a PARACEST agent (5,7) for temperature sensing (9). In vitro results are used to corroborate that CEST attributes are fully conserved while BIRDS properties are detected to enable the possibility that qualitative MR contrast with CEST can be calibrated using quantitative MR mapping with BIRDS. These types of agents with dual CEST and BIRDS properties provide an opportunity for quantitative molecular imaging at high spatial resolution.

Materials and Methods

BIRDS experiments with EuDOTA-$(gly)_4^-$

To assess the BIRDS properties of EuDOTA-$(gly)_4^-$, a database composed of ^1H spectra as a function of temperature was compiled by studying samples of EuDOTA-$(gly)_4^-$ (5 mM) at different pH values (6.5– 8.0) in phosphate buffer (5 mM). The ^1H MRS data of EuDOTA-$(gly)_4^-$ were acquired on an 11.7T Bruker vertical-bore spectrometer at temperatures between 26 and 40 °C using a recycle time (TR) suitable for short relaxation times of these types of agents (Fig. 1A). The correct temperature calibration of the RF probe's thermocouple was verified by two additional methods. The first method was based on chemical shift difference between the -OH and -CH_3 resonances of deuterated methanol (Sigma-Aldrich, No. 343803-5G) (25). For the second method, a thermocouple wire was immersed directly into the solution of the NMR tube. The temperatures measured by both methods in the 26 to 40 °C range were within ±0.5% of the temperature indicated by the probe's thermocouple. The small fluctuation in the values of measured temperatures is very likely due to inherent errors associated with each temperature measurement technique. For the deuterated methanol method, propagation of errors shows that a 1 Hz error in the measurement of the chemical shift difference results in 0.2 °C error in temperature. Moreover, deviation from lorentzian lineshapes of both -OH and -CH_3 resonances, albeit with good shimming at the different temperatures measured, suggests the existence of temperature gradients within the sample, probably due to non-uniform heating/cooling processes. The existence of this temperature gradient could also contribute to the measured temperature for the thermocouple method. [R1.1] The pH in each sample was measured by a Corning 430 pH-meter with a Beckman glass electrode (5 ×178 mm, Calomel). The spectra were line-broadened (10 Hz) and then baseline (first order) and phase (zero order) corrected. The assignments for proton resonances were obtained by a 2D Correlation Spectroscopy (COSY) experiment. The chemical shifts were measured after each resonance was fitted to a Lorentzian lineshape. Longitudinal (T_1) and transverse (T_2) relaxation times of each proton

were measured at 35 °C using conventional inversion recovery and spin echo methods, respectively. T_1 and T_2 values were obtained by fitting the time dependent intensities to a single exponential. For the temperature calibration with EuDOTA-$(gly)_4^-$, the most sensitive non-exchangeable proton was chosen and absolute temperature, T_c, was calculated using its variations in chemical shift, δ_x, according to:

$$T_c = a_0 + a_1(\delta_x - \delta_0) + a_2(\delta_x - \delta_0)^2 \quad [1]$$

where δ_o was set to 20.0 ppm and the coefficients a_0, a_1, and a_2 were determined from linear least-squares fit of measured temperature as a function of chemical shift. [R3.3] [R3.4] The calculated temperature values, T_c, by eq. [1] were later compared with independently measured temperature values, T_m, using a thermocouple wire located around the RF coil reflecting the sample's temperature (see eq. [4]).

The effect of signal-to-noise ratio (SNR) [R3.5] of a resonance on temperature determination was assessed by addition of uniformly distributed random noise of varying amplitudes to the original FID prior to Fourier transformation (23). Baseline (first order) and phase (zero order) corrections were applied to the spectrum and the peak of interest was fitted to a Lorentzian lineshape. The SNR was calculated from the "signal" and "noise" values using the equation (26)

$$SNR = 20 \times log_{10}\left(\frac{signal}{noise}\right) \quad [2]$$

where the "signal" was given by the height of the resonance and the "noise" was estimated from the standard deviation of the signal in a region away from any resonance. For each noise amplitude 100 different runs were used to estimate the corresponding average SNR value and to measure the H4 chemical shifts. Using these chemical shifts, the corresponding temperatures were calculated using eq. [1]. The standard deviation in temperature, σ_T, was estimated for each SNR value from the temperature values obtained during each of the 100 runs.

CEST experiments with EuDOTA-$(gly)_4^-$

CEST properties are based on acquisition of Z-spectra which are frequency dependent saturation spectra (27,28). The ratio M/M_o, which represents the intensity of the bulk water resonances at a certain saturation frequency (i.e., M with RF saturation "on") vs. intensity of the bulk water with saturation frequency at −100 ppm (i.e., M_o, with RF saturation "off"), was plotted against the frequency of the RF saturation pulse to obtain the Z-spectra. [R1.3] Thus, at each frequency of the RF saturation pulse applied, the fractional decrease in the intensity of the bulk water signal was reported, where the intensity of the signal was given by the amplitude of the bulk water resonance. [R1.5] All Z-spectra were acquired on the same 11.7T Bruker vertical-bore spectrometer as all data acquired for BIRDS. The samples contained EuDOTA-$(gly)_4^-$ (5 – 50 mM) and 10% D_2O. A continuous wave RF irradiation of 1 s was used for saturation of various frequencies to obtain the Z-spectra. For the temperature dependence, a sample of 5 mM EuDOTA-$(gly)_4^-$ at pH 7.42 was used and the temperature was varied between 25 and 40 °C. For the pH dependence, samples of 5 mM EuDOTA-$(gly)_4^-$ at 30 °C were used with the pH in the range of 6.5 to 8.0. For the agent concentration dependence, samples at 30 °C were used with EuDOTA-$(gly)_4^-$ concentrations in the range of 5 to 50 mM. For the TR dependence, a sample of 10 mM EuDOTA-$(gly)_4^-$ at pH of 7.0 at 30 °C was used and TR was varied from 1 to 10 s, where the presaturation pulse of 1 s was kept constant. Each ^1H spectrum was line-broadened (5 Hz) and then baseline (first order) and phase (zero order) corrected. The intensity of the bulk

water resonance was measured at each RF saturation frequency and the Z-spectra were generated.

Combined CEST and BIRDS experiments with EuDOTA-$(gly)_4^-$

The phantom used for in vitro imaging experiments consisted of a glass tube containing 20 mM EuDOTA-$(gly)_4^-$ in 10% D_2O at pH 7.0. The CEST data were acquired in ^1H MRI format, whereas the ^1H MRS data for BIRDS were acquired in 2D chemical shift imaging (CSI). The CSI and MRI data, of similar slice position (sample center) and width (2 mm), were acquired on a modified 11.7T Bruker horizontal-bore spectrometer using a ^1H surface coil RF probe (1.4 cm diameter). The ambient temperature was controlled using a water-heating blanket wrapped around the phantom but positioned such that enough space (1–2 cm) was left between the phantom and the blanket. The phantom's temperature was measured by a thermocouple wire (~100 μm diameter, copper-constantan; ±0.05 °C; Oxford Optronix) positioned at the bottom.

For CSI experiments, a field-of-view of 2.56×2.56 cm^2 was used with 32×32 phase encoding steps. A 1 ms Gaussian [R1.C] excitation pulse was used for selective excitation of the most sensitive non-exchangeable proton resonance. The phase-encode gradient duration was 100 μs and the TR was 60 ms. Two different CSI datasets were obtained. One at room temperature (~22 °C) with the water bath turned off and the second with the water bath temperature at 60 °C which resulted in an ambient temperature around the sample of ~42 °C. The spectra were processed as described above for the temperature calibration experiments.

The MRI experiments were acquired using a spin-echo imaging sequence. The imaging parameters were TR of 6 s, echo time of 10 ms, field-of-view of 16×16 mm^2, and image matrix of 128×128. A 1 s square pulse was used for pre-saturation of the bound water prior to the beginning of the spin-echo sequence. At each ambient temperature two images were acquired, one with the saturation offset at the frequency of the bound water resonance (24 kHz, "on" saturation), and the other with the saturation offset on the opposite side of bulk water resonance (−24 kHz, "off" saturation). We used a single saturation frequency of 24 kHz for both temperatures because the bound water peak is very broad, with linewidths much larger than the temperature induced shift of the water bound peak. Moreover, the use of a single saturation frequency bypasses the requirement of measuring the position of the bound water peak before each imaging experiment. [R3.6] For each voxel, the fractional decrease in the intensity of the bulk water signal, M, was reported according to

$$M = 1 - M_{on} \Big/ M_{off} \qquad [3]$$

where M_{on} and M_{off} represent the bulk water intensities for the "on" and "off" saturation experiments, respectively. [R1.3]

Results

Characterization of EuDOTA-$(gly)_4^-$ with BIRDS

A ^1H spectrum of EuDOTA-$(gly)_4^-$ (Fig.1A) shows that its resonances span a relatively wide chemical shift range, of ~40 ppm, although this range is far less wide compared to other Tm^{3+}-based agents like $TmDOTP^{5-}$ and $TmDOTMA^-$ (23,24). Each ^1H resonance, exchangeable or not, was assigned based on a 2D COSY experimental result (data not shown). There are two exchangeable protons observed with EuDOTA-$(gly)_4^-$. First, the bound water signal, better visualized at lower temperature of ~10 °C or so, is located at ~60 ppm from bulk water (Fig. 1A, inset spectrum). Second, the H7 proton belongs to an amide group (Fig. 1A, inset structure). The remaining protons are all non-exchangeable with

variable degrees of sensitivity to temperature and relaxation times (Table 1). While several non-exchangeable protons show variable degree of temperature sensitivity without any noteworthy pH dependency, the H4 proton has the highest temperature sensitivity and good separation from other resonances (Fig. 1A). Linewidths of the EuDOTA-$(gly)_4^-$ protons, at 35 °C and pH of 7.42, are 50 to 70 Hz, with the H4 proton resonance having the largest value. Under these conditions, the temperature sensitivities of the EuDOTA-$(gly)_4^-$ protons are in the range of 0.005 to 0.13 ppm/°C, where again the H4 proton has the highest value. These data pointed to the use of the H4 proton to provide the early temperature characterization of EuDOTA-$(gly)_4^-$ with BIRDS. Thus the absolute temperature, T_c, was calculated from the chemical shift of H4 proton signal as δ_x in eq. [1] using fitted values of the coefficients a_0, a_1, and a_2 (Table 2).

Using error propagation (29) it can be shown that the uncertainties in temperature (ε_T) are proportional to the chemical shift uncertainties (ε_δ): $\varepsilon_T = 7.74\times \varepsilon_\delta$. A very high correlation coefficient (R=0.99998) between the calculated temperature, T_c, and the thermocouple measured temperature, T_m, was obtained by linear least-square fit, as shown by the following linear equation with an intercept close to zero and a slope of unity.

$$T_c=(-0.01 \pm 0.06)+(1.000 \pm 0.002)\cdot T_m \quad [4]$$

To verify the accuracy of temperature determination, as described by eq. [4], we employed an alternative cross-validation method, the “leave one out” method. In this method, the temperature calibration described by eq. [1] was done using a dataset without one of the temperature-chemical shift data points. Then this data-point was used to evaluate the accuracy of the method by calculating the temperature corresponding to the chemical shift data point not used for calibration. The same procedure was repeated for each data-point and the correlation between the calculated temperature using the “leave one out” method, $T_c^{(1out)}$, and the measured temperature T_m, was determined:

$$T_c^{(1out)}=(-0.02 \pm 0.08)+(1.001 \pm 0.002)\cdot T_m \quad [5]$$

Since eqs. [4] and [5] are very similar (i.e., each with a very high correlation coefficient, an intercept close to zero, and a slope of unity), these results indicate that EuDOTA-$(gly)_4^-$ is a very good temperature probe for BIRDS. [R1.2] At 11.7T, for a 5 mM sample of EuDOTA-$(gly)_4^-$ at 35 °C and pH of 7.0, all of the non-exchangeable protons have T_1’s and T_2’s in the range of 30 to 150 ms and 5 to 10 ms, respectively (Table 1). This indicates that a short TR can be used for 2D CSI data acquisition needed for BIRDS.

Repeated simulations of temperature determination using the H4 chemical shift (eq. [1]) but with different SNR were used to address the question of how the error of temperature measurement (σ_T) depends on the SNR (23). The error of the temperature prediction was estimated by means of the temperature standard deviations for 100 runs at a given SNR value (Fig. 1C). Typical in vitro SNR values for the H4 proton are in the range 10 to 30 for a 0.8×0.8×2 mm^3 voxel. This SNR range corresponds to a temperature standard deviation of less than 0.07 °C (Fig. 1C). Similar standard deviations in temperature (0.06 °C) were obtained using the N-acetyl aspartate (NAA) and water method, but for a much larger voxel size of 1.6×1.6×4 mm^3 (23). Therefore EuDOTA-$(gly)_4^-$ with BIRDS is at least as good as the NAA-water method for temperature determination with the potential of considerably higher spatial resolution (23,24). Temperature accuracy (by BIRDS) as function of SNR was previously estimated for two other Tm^{3+}-based agents, $TmDOTP^{5-}$ and $TmDOTMA^-$ (23,24). The temperature standard deviation in a spectrum of a CSI voxel acquired under identical experimental conditions (i.e., volume, acquisition time, agent concentration) is 0.01 °C for EuDOTA-$(gly)_4^-$ at SNR = 25 (Fig. 1C) and 0.008 and 0.002 °C, respectively, for

$TmDOTP^{5-}$ and $TmDOTMA^{-}$ (23). Thus, the accuracy of temperature determination with EuDOTA-$(gly)_4^{-}$ is comparable to that with $TmDOTP^{5-}$, but slightly lower than with $TmDOTMA^{-}$.

Characterization of EuDOTA-$(gly)_4^{-}$ with CEST

Since it is well known that CEST contrast depends on many experimental factors (e.g., B_o inhomogeneity, temperature and/or pH around the agent, agent concentration, TR of CEST experiment, etc.) (1,2), we acquired Z-spectra of EuDOTA-$(gly)_4^{-}$ under various experimental conditions to characterize its CEST properties (Fig. 2). EuDOTA-$(gly)_4^{-}$ is a well known PARACEST agent for temperature mapping (5,7,9). The CEST effect from the exchangeable water molecule increases with an increase in temperature (Fig. 2A). CEST is more efficient at higher temperatures because exchange of water molecules between the two pools is faster. Above ~40 °C, however, the CEST effect begins to decline once again because water exchange becomes too fast (30). We note that the frequency at which the M/M_o ratio has a minimum, corresponding to the frequency of the bound water signal, is also temperature-dependent with a sensitivity of about −0.22 ppm/°C at 35 °C. However, this broad water signal has an SNR which is an order of magnitude lower than the other non-exchangeable protons (Fig. 1A), thereby reducing accuracy of temperature determination. [R3.1] The increase in temperature also results in broadening of both the bound and bulk water peak profiles in the Z-spectra.

The effect of pH is not as significant as that for temperature with EuDOTA-$(gly)_4^{-}$. Changing pH between 6.5 and 8.0 has a small effect on CEST from bound water exchange (Fig. 2B). The relatively minor changes in M/M_o likely reflect the four pH dependent –NH protons in the complex that are also exchanging with solvent protons. This exchange, although not observed directly in the Z-spectrum, effectively shortens the T_2 of bulk water (31). Water exchange in PARACEST agents in general does not depend on pH but other exchangeable functional groups in these complexes may potentially be used as pH sensitive CEST sites (32).

Changing the concentration of EuDOTA-$(gly)_4^{-}$ by an order of magnitude produces the largest change in CEST (Fig. 2C). Note that, due to 10% D_2O content in each sample, the actual concentration of EuDOTA-$(gly)_4^{-}$ agent which contributes to CEST effect is only 90% of the total agent concentration. The magnitude of the CEST effect does not increase linearly with concentration at the levels examined here because one approaches maximal CEST (i.e., M/M_o approaches 0) at agent concentrations higher than 45 mM. [R1.4] These data do illustrate that the magnitude of CEST is highly concentration dependent, a problem common to both PARACEST and DIACEST agents for in vivo applications (1,2).

The Z-spectra also exhibit a small dependence on TR, with shorter TR values giving a somewhat larger CEST effect (i.e., smaller M/M_o) (Fig. 2D). In acquisition of these data the saturation pulse of 1 s was kept constant and only TR was changed. Although the reason for this observation may not be obvious, this reflects incomplete relaxation of bulk water protons between scans using a relatively short saturation pulse length (1 s) and a short TR so the steady-state level of saturation is achieved that result in a larger net CEST effect. One should also notice that the bound water exchange resonance in the Z-spectra at short TR are broader than those at higher TR (Fig. 2D). These data illustrated that one can achieve good CEST contrast without conducting CEST experiments under fully relaxed conditions.

Dual characterization of EuDOTA-$(gly)_4^{-}$ with BIRDS and CEST imaging

Temperature distributions of a cylindrical glass phantom were examined by BIRDS and CEST imaging with an identical slice location and thickness (Fig. 3). A representative voxel

from the CSI grid (Fig. 3A) shows a high SNR for the H4 proton (Fig. 3B) which shifts with a temperature sensitivity of about −0.13 ppm/°C and has negligible pH dependency (Fig. 1B; Table 1). The absolute temperature in each voxel of the CSI dataset was calculated according to eq. [1] at two different ambient conditions. With BIRDS, the average temperature in the phantom was 22.1±0.1 °C with the water bath turned off (Fig. 3C, left) and 41.6±0.1 °C with the water bath turned on (Fig. 3C, right). This agreed well with temperatures measured using a thermocouple wire (i.e., ~22 °C and ~42 °C for the water bath turn off and on, respectively).

Two spin-echo MRI data sets with CEST contrast were also obtained at these two ambient conditions (Fig. 3D). The change in the intensity of the bulk water signal after pre-saturation of the bound water was calculated relative to the bulk water signal in the absence of saturation according to eq. [3]. The upper half of the MRI datasets with higher SNR values was used and regions of poor RF sensitivity farther away from the surface coil (i.e., B_1 inhomogeneity) were excluded. With CEST, the results indicate that the average intensity change in the phantom was 15±3% (Fig. 3D, left) and 32±7% (Fig. 3D, right), with the water bath turned off and on, respectively.

To estimate the RF heating of the sample caused by rapid RF pulsing, we repeated both CSI and MRI experiments with a thermocouple wire inserted inside the NMR tube, positioned in the center of the region from where the MR signal was acquired. Due to high B_0 inhomogeneities induced by the presence of the thermocouple, simultaneous MR data acquisition and temperature measurement by thermocouple was not possible. The average temperature increase during a 4.5 minutes long CSI experiment was 0.024±0.019 °C, while for a 7 minute MRI sequence with CEST contrast, the average temperature increase was 0.3±0.1 °C. [R1.10]

Discussion

Here we report that EuDOTA-$(gly)_4^-$ possesses dual CEST and BIRDS properties which could potentially improve quantitative biosensing. EuDOTA-$(gly)_4^-$ is a tetraglycinate derivative of the macrocyclic chelate $DOTA^{-4}$ and it has been shown to be a PARACEST agent for temperature (5,7,9). The bound water lifetime in EuDOTA-$(gly)^{4-}$ was estimated to be around 300 μs at 298 K (7). However the CEST efficiency of an agent is given by the product between the bound water lifetime (τ_M) and the chemical shift separation ($\Delta\omega$) between the bound and bulk water peaks (31). EuDOTA-$(gly)_4^-$ has a $\Delta\omega\tau_M$ value in range of ~7.7 at 1.5T and ~60 at 11.7T, where a higher $\Delta\omega\tau_M$ values suggests a more efficient CEST effect (1,2). [R1.8] Thus LnDOTA-$(gly)_4^-$ is likely to be a more efficient PARACEST agent at higher B_o, although it could still be effective at low B_o (33) but the CEST efficiency may drop by nearly an order of magnitude from 11.7T to 1.5T. These measured CEST properties of EuDOTA-$(gly)_4^-$ are manifested by proton exchange between bulk water and bound water pools (Fig. 1A, inset spectrum), but the H7 amide proton of EuDOTA-$(gly)_4^-$ (Fig. 1A, inset structure) is another exchangeable pool which could be exploited further for additional CEST effects and remain to be investigated in future studies.

The remaining 8 proton signals emanating from the backbone of the $DOTA^{-4}$ chelate (Fig. 1A) do not exchange and therefore are readily detectable by conventional ^1H MRS. Detection by BIRDS is improved if the relaxation properties (Table 1) are exploited to allow short TR experiments with high speed CSI. A variation in pH has little effect on chemical shifts of these protons. Chemical shifts of the protons are sensitive mainly to temperature variations and amongst all of these protons H4 is the most sensitive (Table 1). Thus we propose a second-order dependence between temperature and the H4 chemical shift, as described by eq. [1], because pH dependency can be ignored within the physiological range

(Fig. 1B). This allows a measure of temperature with quite high accuracy. For a CSI voxel of 0.8×0.8×2.0 mm^3 (as used in this study with SNR in the range of 10 to 30 for the H4 signal) the error in temperature prediction is less than 0.07 °C (Fig. 1C; Table 2). This level of uncertainty in temperature prediction using EuDOTA-$(gly)_4^-$ with BIRDS compares quite well with other temperature mapping methods, e.g., the NAA-water method or $TmDOTP^{5-}$ with BIRDS (23). However we used only 1 proton resonance of EuDOTA-$(gly)_4^-$ (i.e., H4; see Table 1) for temperature prediction. If some of the other proton resonances of EuDOTA-$(gly)_4^-$ (e.g., H5 and H6, both of which have comparable temperature sensitivities (see Table 1) are also used – as with $TmDOTP^{5-}$ where 3 proton resonances are used (23) – the redundancy of information contained within the biosensor could be improved to reduce the uncertainty in temperature even further. We envisage then that uncertainty in temperature prediction using EuDOTA-$(gly)_4^-$ with 3 proton resonances (i.e., H4–H6; see Table 1) may compare quite well with temperature sensitivity of $TmDOTMA^-$ with BIRDS (24).

The CEST contrast is based on transfer of magnetization via proton exchange from the exchangeable solute pool to the bulk water pool and the effect can be observed if the system is in "slow exchange" or $\Delta\omega\tau_M \geq 1$. Therefore an agent with a relatively large $\Delta\omega$ is better because it provides a CEST effect even with a short τ_M. In addition, as pointed out earlier, the much larger chemical shift separation between signals arising from the pools of exchangeable protons availed by PARACEST agents (vs. DIACEST agents) reduce the vulnerability of CEST contrast to B_o inhomogeneity (i.e., poor shim). However for the CEST effect of EuDOTA-$(gly)^{4-}$ to be easily quantifiable, the MRI contrast needs to respond specifically to temperature (Fig. 2A) and not to other experimental factors (Figs. 2B–D). A primary concern for quantitative CEST contrast is the dependence of the effect on agent concentration (Fig. 2C). Although pH and TR effects on the M/M_o ratio for EuDOTA-$(gly)^{4-}$ are small (Figs. 2B and 2D), they may not be ignored with other PARACEST agents. Another issue of concern for CEST contrast that needs further study is B_1 inhomogeneity (e.g., with RF surface coil), as observed in the CEST imaging data (Fig. 3D).

In vitro CEST imaging showed ~15% and ~30% contrast in the MRI data with the water bath turned off (Fig. 3D, left) and on (Fig. 3D, right) which respectively corresponded to ~22 °C (Fig. 3C, left) and ~42 °C (Fig. 3C, right) measured by BIRDS and thermocouple wires. However additional information is needed to convert the qualitative MRI intensity change from CEST imaging to actual temperature values. First and foremost, it is obligatory to know the concentration of EuDOTA-$(gly)_4^-$. In addition, it is also necessary to negate any affects on the MRI intensity change due to contributions from B_o inhomogeneity, B_1 inhomogeneity, TR effects, and/or pH effects. While in this study we have shown the effect of TR and pH on CEST quantification with EuDOTA-$(gly)_4^-$, the experimental conditions were not ideal for examining the effects of B_0 and B_1 inhomogeneities because we used ideal B_0 shim conditions and used an RF surface coil which SNR variations. Future studies will quantitatively assess the impact of B_0 and B_1 inhomogeneities on the CEST effect with EuDOTA-$(gly)_4^-$. [R1.6] [R1.7]

Based primarily on information obtained from $TmDOTP^{5-}$ and $TmDOTMA^-$, BIRDS quantification is not as susceptible to many of these experimental factors (23,24). Physiological information extracted from the CSI data, and thus BIRDS, is inherently independent of the agent concentration (i.e., beyond detection limit). Since physiological quantification is dependent on the non-exchangeable resonance chemical shifts and not intensity, inherent B_1 inhomogeneity present in MRI or MRS data with RF surface coils is much less of a concern for BIRDS. Furthermore physiological quantification (e.g., temperature, pH, etc) based on shifts of the non-exchangeable protons are nearly constant across different B_o's, thus enabling BIRDS properties to be nearly B_o-independent. Because

T_2/T_1 ratios of these protons are quite constant across different B_o's, at nominal TR values only marginal SNR loss is expected at a lower vs. higher B_o. In fact, for some agent designs it is even possible to reach T_2/T_1 ratios of close to unity thus allowing optimal sensitivity of detection since then SNR is directly proportional to $\sqrt{T_2/T_1}$. The extremely short T_2's of the non-exchangeable protons make their detection, and thus BIRDS, nearly impervious to B_o inhomogeneity. Furthermore BIRDS can easily measure the ambient conditions of the agent (i.e., temperature and/or pH). All of these benefits from BIRDS could be used to improve quantitative imaging with CEST. For example, BIRDS can be used to measure the distribution of both sample temperature and agent concentration. Using these measurements, the CEST experiment may be corrected for temperature and/or agent concentration effects to accurately measure another physiological parameter, such as pH. [R1.9] Recently, a new MRI-based method by Dixon et al (30) has been proposed which quantifies the CEST effect of a PARACEST agent with multi-parametric modeling, thereby negating the need for the agent's concentration. It would be extremely important to compare the accuracies of dual biosensing with BIRDS-CEST vs. the Dixon method for molecular imaging applications. [R3.2]

Another advantage of EuDOTA-$(gly)_4^-$ is that it has the potential for translation to in vivo studies. Pharmacokinetics studies on rats injected with 100 μL solution of EuDOTA-$(gly)_4^-$ containing traces of radioactive lutetium III ion ($^{177}Lu^{3+}$) in the form of ^{177}LuDOTA-$(gly)_4^-$ indicate an average elimination half-life of 20 minutes (15). Biodistribution measurements show that 30 minutes after the injection the residual ^{177}LuDOTA-$(gly)_4^-$ was localized mainly in blood, kidney, and urine, whereas 2 hours later the ^{177}LuDOTA-$(gly)_4^-$ levels decreased significantly due to rapid excretion. Toxicity studies of EuDOTA-$(gly)_4^-$ showed that a relatively high dose (1 mmol/Kg) [R1.D] was well tolerated with minimal effect on the health of the animal. Although EuDOTA-$(gly)_4^-$ has a relatively low thermodynamic stability compared to other agents containing gadolinium (III) ion (i.e., Gd^{3+}), e.g., GdDOTA (Dotarem), it exhibits a relatively high kinetic stability which represents the major factor in determining the toxicity of any Ln^{3+}-based agent. However, in vivo studies with EuDOTA-$(gly)_4^-$ may require that the agent remain in circulation for several hours during accumulation of the MR data, perhaps aided by renal ligation (22–24). In that case, additional toxicity measurements coupled with SNR estimation in vivo under renal ligation conditions will be required to correctly estimate the optimal in vivo dose needed for EuDOTA-$(gly)_4^-$ in rats, as previously done for $TmDOTP^{5-}$ and $TmDOTMA^-$ (23,24). Moreover, the use of relatively high saturation powers during CEST experiments may result in slight heating of the sample investigated. Although the temperature increase observed during the CEST experiment in this study were quite small (<0.3°C), special attention needs to be employed during eventual pre-clinical as well as clinical applications using CEST imaging. [R1.10] [R1.11] A further issue for pre-clinical and clinical applications will be exclusion of B_0 and B_1 inhomogeneities on the CEST effect. For the latter concern, however, BIRDS could be used to potentially circumvent because it is less affected by B_0 and B_1 inhomogeneities. [R1.11]

Conclusions

Using EuDOTA-$(gly)_4^-$ we obtained temperature data (measured by BIRDS) at two different ambient conditions within 0.1 °C accuracy of the actual temperature of the phantom (measured by thermocouple). Quantitative information from BIRDS obtained at CSI spatial resolution (i.e., voxel size of 0.8×0.8×2.0 mm^3) may be used to improve the qualitative CEST contrast which has higher MRI spatial resolution (i.e., voxel size of 0.125×0.125×2.0 mm^3) but may suffer from unknown contributions from various experimental factors. These results suggest that EuDOTA-$(gly)_4^-$ and other PARACEST-

like agents which possess high numbers of exchangeable and non-exchangeable protons can be used as a dual biosensor featuring both CEST and BIRDS properties. Future studies should seek agent designs that enhance BIRDS sensitivity without diminishing the advantages of CEST as these combined properties in a single molecular probe can have a wide range of MRI and MRS applications in functional brain studies (34–38).

Abbreviations

BIRDS	biosensor imaging of redundant deviation in shifts
CEST	chemical exchange saturation transfer
DIACEST	diamagnetic CEST
MR	magnetic resonance
MRI	magnetic resonance imaging
MRS	magnetic resonance spectroscopy
PARACEST	paramagnetic CEST
SNR	signal-to-noise ration
RCAs	responsive contrast agents

Acknowledgments

The authors thank scientists and engineers at MRRC (mrrc.yale.edu), and QNMR (qnmr.yale.edu). This work was supported by grants from National Institutes of Health (R01 MH-067528 to FH, R01 CA-140102 to FH/GEK, R01 EB-011968 to FH, R01 AG-034953 to DLR, P30 NS-52519 to FH, R01 CA-115531 to ADS, R01 EB-004582 to ADS, and P41 RR-002584 to ADS).

References

1. Zhou J, van Zijl PC. Chemical exchange saturation transfer imaging and spectroscopy. Prog Nucl Magn Reson Spec. 2006; 48:109–136.
2. Sherry AD, Woods M. Chemical exchange saturation transfer contrast agents for magnetic resonance imaging. Annu Rev Biomed Eng. 2008; 10:391–411. [PubMed: 18647117]
3. Ward KM, Aletras AH, Balaban RS. A new class of contrast agents for MRI based on proton chemical exchange dependent saturation transfer (CEST). J Magn Reson. 2000; 143(1):79–87. [PubMed: 10698648]
4. Zhang S, Wu K, Sherry AD. Unusually sharp dependence of water exchange rate versus lanthanide ionic radii for a series of tetraamide complexes. J Am Chem Soc. 2002; 124(16):4226–4227. [PubMed: 11960448]
5. Aime S, Barge A, Delli Castelli D, Fedeli F, Mortillaro A, Nielsen FU, Terreno E. Paramagnetic lanthanide(III) complexes as pH-sensitive chemical exchange saturation transfer (CEST) contrast agents for MRI applications. Magn Reson Med. 2002; 47(4):639–648. [PubMed: 11948724]
6. Aime S, Barge A, Gianolio E, Pagliarin R, Silengo L, Tei L. High relaxivity contrast agents for MRI and molecular imaging. Ernst Schering Res Found Workshop. 2005; (49):99–121. [PubMed: 15524213]
7. Zhang S, Sherry AD. Physical characteristics of lanthanide complexes that act as magnetization transfer (MT) contrast agents. Journal of Solid State Chemistry. 2003; 171(1–2):38–43.
8. Li AX, Wojciechowski F, Suchy M, Jones CK, Hudson RH, Menon RS, Bartha R. A sensitive PARACEST contrast agent for temperature MRI: Eu3+DOTAM-glycine (Gly)-phenylalanine (Phe). Magn Reson Med. 2008; 59(2):374–381. [PubMed: 18228602]
9. Zhang S, Malloy CR, Sherry AD. MRI thermometry based on PARACEST agents. J Am Chem Soc. 2005; 127(50):17572–17573. [PubMed: 16351064]

10. Aime S, Delli Castelli D, Fedeli F, Terreno E. A paramagnetic MRI-CEST agent responsive to lactate concentration. J Am Chem Soc. 2002; 124(32):9364–9365. [PubMed: 12167018]
11. Zhang S, Trokowski R, Sherry AD. A paramagnetic CEST agent for imaging glucose by MRI. J Am Chem Soc. 2003; 125(50):15288–15289. [PubMed: 14664562]
12. Ren J, Trokowski R, Zhang S, Malloy CR, Sherry AD. Imaging the tissue distribution of glucose in livers using a PARACEST sensor. Magn Reson Med. 2008; 60(5):1047–1055. [PubMed: 18958853]
13. Dhingra K, Maier ME, Beyerlein M, Angelovski G, Logothetis NK. Synthesis and characterization of a smart contrast agent sensitive to calcium. Chem Commun (Camb). 2008; 7(29):3444–3446. [PubMed: 18633517]
14. Esqueda AC, Lopez JA, Andreu-de-Riquer G, Alvarado-Monzon JC, Ratnakar J, Lubag AJ, Sherry AD, De Leon-Rodriguez LM. A new gadolinium-based MRI zinc sensor. J Am Chem Soc. 2009; 131(32):11387–11391. [PubMed: 19630391]
15. Sherry AD, Caravan P, Lenkinski RE. Primer on Gadolinium Chemistry. Journal of Magnetic Resonance Imaging. 2009; 30(6):1240–1248. [PubMed: 19938036]
16. Aime S, Botta M, Fasano M, Marques MP, Geraldes CF, Pubanz D, Merbach AE. Conformational and Coordination Equilibria on DOTA Complexes of Lanthanide Metal Ions in Aqueous Solution Studied by (1)H-NMR Spectroscopy. Inorg Chem. 1997; 36(10):2059–2068. [PubMed: 11669824]
17. Geraldes CFGC, Sherry AD, Kiefer GE. The solution structure of Ln (DOTP)5- complexxes. A comparison of lanthanide-induced paramagnetic shifts with the MMX energy-minimized structure. Journal of Magnetic Resonance. 1992; 97(2):290–304.
18. Sherry AD, Ren J, Huskens J, Brucher E, Toth E, Geraldes CFCG, Castro MMCA, Cacheris WP. Characterization of Lanthanide(III) DOTP Complexes: Thermodynamics, Protonation, and Coordination to Alkali Metal Ions. Inorganic Chemistry. 1996; 35(16):4604–4612.
19. Pasha A, Lin M, Tircso G, Rostollan CL, Woods M, Kiefer GE, Sherry AD, Sun X. Synthesis and evaluation of lanthanide ion DOTA-tetraamide complexes bearing peripheral hydroxyl groups. J Biol Inorg Chem. 2009; 14(3):421–438. [PubMed: 19083028]
20. Zuo CS, Bowers JL, Metz KR, Nosaka T, Sherry AD, Clouse ME. TmDOTP5-: a substance for NMR temperature measurements in vivo. Magn Reson Med. 1996; 36(6):955–959. [PubMed: 8946362]
21. Bansal N, Germann MJ, Lazar I, Malloy CR, Sherry AD. In vivo Na-23 MR imaging and spectroscopy of rat brain during TmDOTP5- infusion. J Magn Reson Imaging. 1992; 2(4):385–391. [PubMed: 1633390]
22. Trubel HK, Maciejewski PK, Farber JH, Hyder F. Brain temperature measured by 1H-NMR in conjunction with a lanthanide complex. J Appl Physiol. 2003; 94(4):1641–1649. [PubMed: 12626478]
23. Coman D, Trubel HK, Rycyna RE, Hyder F. Brain temperature and pH measured by (1)H chemical shift imaging of a thulium agent. NMR Biomed. 2009; 22(2):229–239. [PubMed: 19130468]
24. Coman D, Trubel HK, Hyder F. Brain temperature by Biosensor Imaging of Redundant Deviation in Shifts (BIRDS): comparison between $TmDOTP^{5-}$ and $TmDOTMA^{-}$. NMR Biomed. 2010; 23(3):277–285. [PubMed: 19957287]
25. Findeisen M, Brand T, Berger S. A 1H-NMR thermometer suitable for cryoprobes. Magn Reson Chem. 2007; 45(2):175–178. [PubMed: 17154329]
26. Morton DW, Maravilla KR, Meno JR, Winn HR. Clinically relevant rat model for testing BOLD functional MR imaging techniques by using single-shot echo-planar imaging at 1.5 T. Radiology. 2001; 218(2):598–601. [PubMed: 11161185]
27. Grad J, Bryant RG. Nuclear magnetic cross-relaxation spectroscopy. Journal of Magnetic Resonance. 1990; 90(1):1–8.
28. Grad J, Mendelson D, Hyder F, Bryant RG. Applications of nuclear magnetic cross-relaxation spectroscopy to tissues. Magn Reson Med. 1991; 17(2):452–459. [PubMed: 2062216]
29. Bevington, PR. Data Reduction and Error Analysis for The Physical Sciences. New York, NY: McGraw-Hill Book Company; 1969. p. 336

30. Dixon WT, Ren J, Lubag AJ, Ratnakar J, Vinogradov E, Hancu I, Lenkinski RE, Sherry AD. A concentration-independent method to measure exchange rates in PARACEST agents. Magn Reson Med. 2010; 63(3):625–632. [PubMed: 20187174]

31. Zhang S, Merritt M, Woessner DE, Lenkinski RE, Sherry AD. PARACEST agents: modulating MRI contrast via water proton exchange. Acc Chem Res. 2003; 36(10):783–790. [PubMed: 14567712]

32. Pikkemaat JA, Wegh RT, Lamerichs R, van de Molengraaf RA, Langereis S, Burdinski D, Raymond AY, Janssen HM, de Waal BF, Willard NP, Meijer EW, Grull H. Dendritic PARACEST contrast agents for magnetic resonance imaging. Contrast Media Mol Imaging. 2007; 2(5):229–239. [PubMed: 17937448]

33. Vinogradov E, He H, Lubag A, Balschi JA, Sherry AD, Lenkinski RE. MRI detection of paramagnetic chemical exchange effects in mice kidneys in vivo. Magn Reson Med. 2007; 58(4): 650–655. [PubMed: 17899603]

34. Trubel H, Herman P, Kampmann C, Novotny E, Hyder F. Selective pharyngeal brain cooling. Biomed Tech (Berl). 2003; 48(11):298–300. [PubMed: 14661532]

35. Trubel H, Herman P, Kampmann C, Huth R, Maciejewski PK, Novotny E, Hyder F. A novel approach for selective brain cooling: implications for hypercapnia and seizure activity. Intensive Care Med. 2004; 30(9):1829–1833. [PubMed: 15185071]

36. Trubel H, Herman P, Kampmann C, Novotny E, Hyder F. Duration of induced seizures during selective pharyngeal brain cooling. Biomed Tech (Berl). 2004; 49(10):279–281. [PubMed: 15566077]

37. Trubel HK, Sacolick LI, Hyder F. Regional temperature changes in the brain during somatosensory stimulation. J Cereb Blood Flow Metab. 2006; 26(1):68–78. [PubMed: 15959461]

38. Maandag NJ, Coman D, Sanganahalli BG, Herman P, Smith AJ, Blumenfeld H, Shulman RG, Hyder F. Energetics of neuronal signaling and fMRI activity. Proc Natl Acad Sci U S A. 2007; 104(51):20546–20551. [PubMed: 18079290]

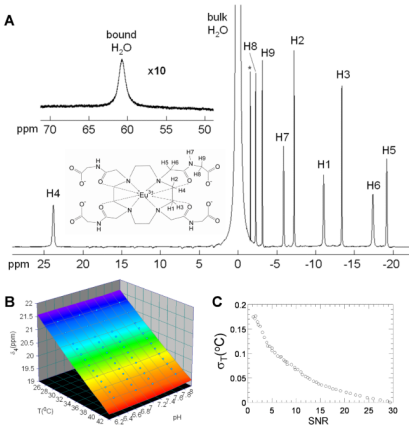

Figure 1. BIRDS characterization of EuDOTA-(gly)$_4^-$

(A) Proton spectrum at pH of 7.0 and temperature of 10 °C. Insets represent the chemical structure of EuDOTA-(gly)$_4^-$ and the bound water resonance at ~60 ppm. The ^{1}H resonances were assigned by 2D COSY data. The resonance marked by * corresponds to traces of an HPLC solvent left in the sample after purification. The H7 proton belongs to the amide. (B) 3D surface plot showing the temperature and pH dependencies of H4 proton chemical shift which is unaffected by pH, thereby simplifying the equation for temperature calibration to a second order polynomial (eq. [1]). (C) Accuracy of temperature determination at various SNR values for the H4 resonance. The SNR of a voxel during a typical in vitro CSI experiment is in the range of 10 to 25, which corresponds to a standard deviation in temperature of 0.07 °C or smaller.

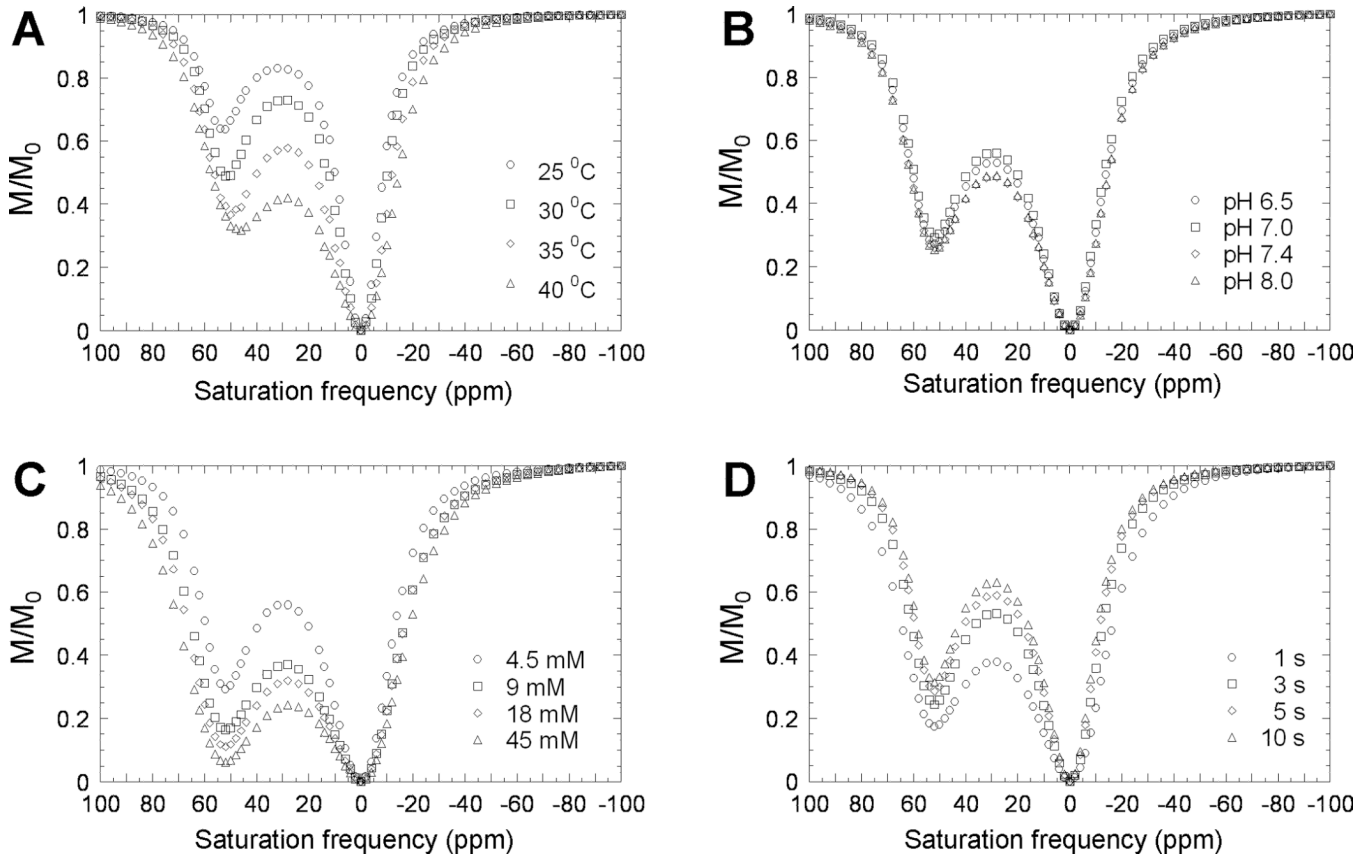

Figure 2. CEST characterization of EuDOTA-(gly)$_4^{-}$

Z-spectra corresponding to effects of (A) temperature, (B) pH, (C) effective agent concentration, and (D) TR. The CEST effects were generated by a selective continuous wave square shaped RF saturation pulse duration of 1 s with a B_1 field of 78 μT. In Fig. 2C, due to 10% D_2O content in each sample, the effective concentration of EuDOTA-(gly)$_4^{-}$ agent which contributes to CEST is 90% of the total agent concentration. [R1.4]

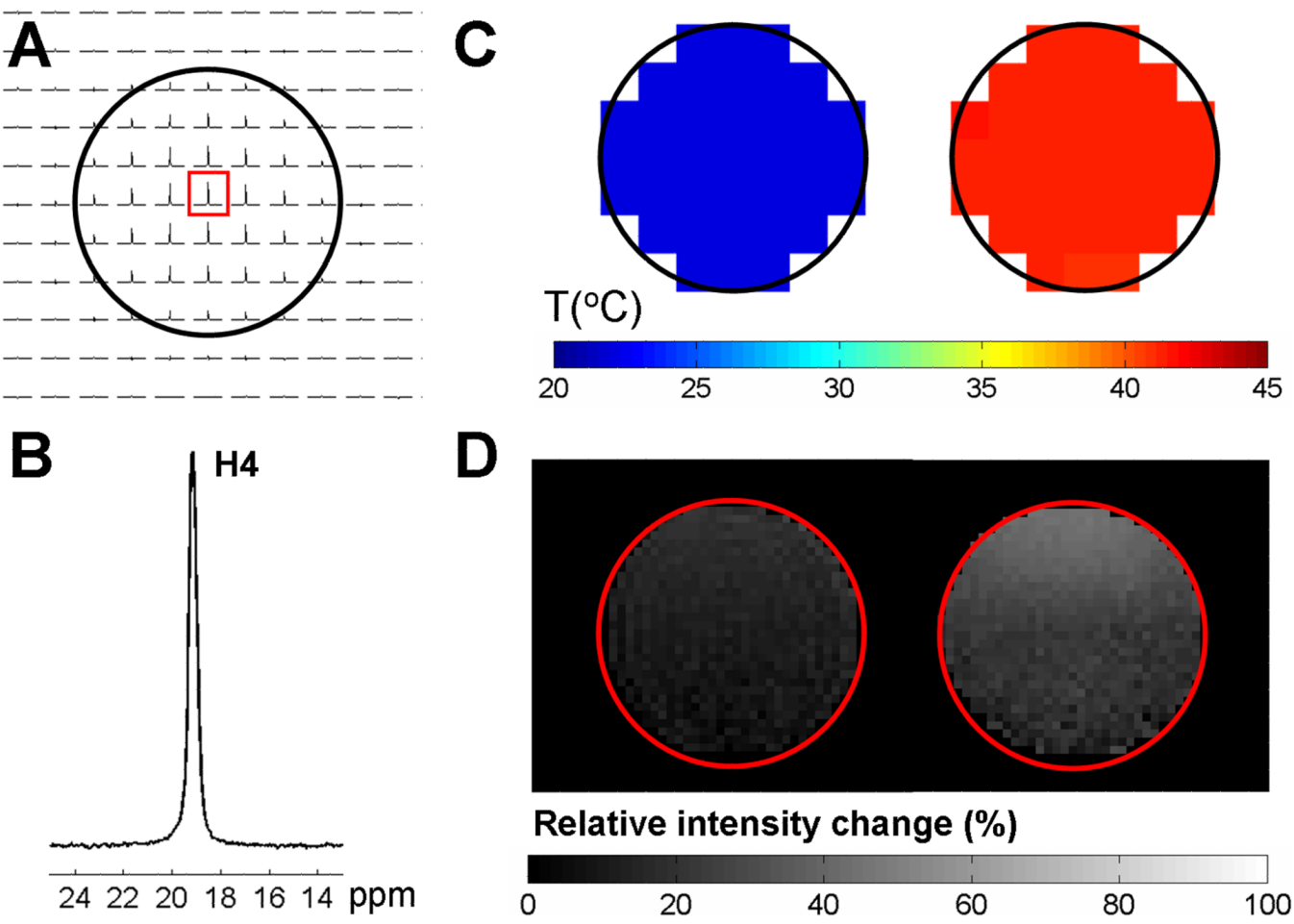

Figure 3. BIRDS and CEST imaging with EuDOTA-(gly)$_4^-$

In vitro temperature effects of a phantom consisting of a cylindrical tube with 20 mM EuDOTA-(gly)$_4^-$ in 10% D_2O at pH 7.0. (A) Proton 2D CSI data set demonstrating the distribution of the H4 resonance on a 2 mm slice of the phantom. The CSI voxel dimension was 0.8×0.8×2 mm^3. (B) Example of proton spectrum from a CSI voxel indicated by a red box in A. (C) In vitro BIRDS. Temperature maps of the phantom obtained by BIRDS at room temperature (left) and heated using a water-heating blanket (right). (D) In vitro CEST. MRI maps obtained under the same two ambient conditions as above (i.e., left represents room temperature, right represents heating by a water-heating blanket), but each image represents the percentage decrease in intensity due to the CEST effect calculated according to eq. [3]. A square shaped RF saturation pulse of 1 s duration and B_1 field of 32.6 μT was used. [R1.10] The CEST contrast is attenuated at the lower temperature as suggested by the Z-spectra in Fig. 2A. However this CEST contrast is not quantitative unless the experimental factors like concentration and pH of EuDOTA-(gly)$_4^-$ as well as the TR are known.

Table 1

Temperature sensitivities and relaxation times for EuDOTA-$(gly)_4^-$ protons (at 35 °C and pH of 7.0).

Proton	Temperature sensitivity (ppm/°C)	T_1 (ms)	T_2 (ms)
H1	0.0593 ± 0.0002	30.9 ± 1.2	5.6 ± 0.3
H2	0.0051 ± 0.0003	38.7 ± 1.3	6.3 ± 0.3
H3	0.0223 ± 0.0003	34.9 ± 0.6	7.0 ± 0.3
H4	−0.1299 ± 0.0003	26.7 ± 1.3	6.2 ± 0.2
H5	0.0754 ± 0.0004	37.1 ± 1.7	7.0 ± 0.5
H6	0.1033 ± 0.0004	29.0 ± 1.0	5.8 ± 0.2
H7[a]	-	-	-
H8	0.0154 ± 0.0004	140.5 ± 5.1	10.2 ± 0.9
H9	0.0242 ± 0.0005	151.6 ± 3.2	6.1 ± 0.5

[a] the H7 amide proton is in fast exchange with the bulk water (observed at temperatures 15 °C).

Table 2

Coefficients a_0, a_1 and a_2 for temperature with H4 resonance of EuDOTA-$(gly)_4^-$.

Coefficient	Value
$\mathbf{a_0}$	35.30 ± 0.01
$\mathbf{a_1}$	−7.74 ± 0.02
$\mathbf{a_2}$	0.32 ± 0.02